Food Chemistry 455 (2024) 139856

Contents lists available at ScienceDirect

Food Chemistry

journal homepage: www.elsevier.com/locate/foodchem

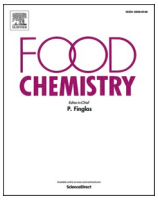

Probing the alterations in mice cecal content due to high-fat diet

Cheherazade Trouki [a,b], Beatrice Campanella [c,*], Massimo Onor [c], Andrea Vornoli [d], Luisa Pozzo [d], Vincenzo Longo [d], Emilia Bramanti [c]

[a] CNR-IPCF, Institute of Chemical and Physical Processes, National Research Council, via Moruzzi 1, Pisa 56124, Italy
[b] Department of Pharmacy, University of Pisa, Via Bonanno 6, Pisa 56126, Italy
[c] CNR-ICCOM, Institute of Chemistry of Organometallic Compounds, National Research Council, via Moruzzi 1, Pisa 56124, Italy
[d] CNR-IBBA, Institute of Agricultural Biology and Biotechnology, National Research Council, Via Moruzzi 1, Pisa 56124, Italy

ARTICLE INFO

Keywords:
Infrared spectroscopy
Chemometrics
Gut microbiota
Metabolism
High fat diet

ABSTRACT

The global prevalence of obesity more than doubled between 1990 and 2022. By 2022, 2.5 billion adults aged 18 and older were overweight, with over 890 million of them living with obesity. The urgent need for understanding the impact of high-fat diet, together with the demanding of analytical methods with low energy/chemicals consumption, can be fulfilled by rapid, high-throughput spectroscopic techniques.

To understand the impact of high-fat diet on the metabolic signatures of mouse cecal contents, we characterized metabolite variations in two diet-groups (standard *vs* high-fat diet) using FTIR spectroscopy and multivariate analysis. Their cecal content showed distinct spectral features corresponding to high- and low-molecular-weight metabolites. Further quantification of 13 low-molecular-weight metabolites using liquid chromatography showed significant reduction in the production of short chain fatty acids and amino acids associated with high-fat diet samples. These findings demonstrated the potential of spectroscopy to follow changes in gut metabolites.

1. Introduction

Evidence, mainly from animal models, suggests that the gut microbiota significantly affects host health (Flint, Scott, Louis, & Duncan, 2012). Diseases linked to diet, such as obesity, are also associated with changes in the gut microbiota. Obesity is indeed not only a matter of calories intake but also of the selection of gut microbiota populations that impact via bacterial metabolites (e.g. short-chain fatty acids, lipopolysaccharides…) on host energy metabolism, inflammation, and regulation of fat deposition and bile acid metabolism.(Breton, Galmiche, & Déchelotte, 2022).

Mice are commonly used in biomedical research because their physiological and anatomical structures, including the gastrointestinal tract, are similar to humans (Nguyen, Vieira-Silva, Liston, & Raes, 2015). Studies on mice fed high-fat diets have shown gut microbiota changes similar to those observed in humans. However, some important differences must be considered. Human studies typically use stool samples, whereas mouse studies use cecal content. The mouse cecum is large and important for fermenting plant materials and producing vitamins K and B, which mice reabsorb by eating their feces. In contrast, the human cecum is smaller, resembles the colon, and lacks a distinct function. While the murine model remains valuable for studying host-microbiota interactions, caution is needed when drawing direct parallels between murine and human gut microbiota compositions (Nguyen et al., 2015).

In mice, the cecum gut portion is an important site of water and electrolyte absorption, but also of digesta retention and microbial fermentation (Breves, 1995; Jandhyala et al., 2015). In this framework, the study of metabolite composition of cecal content under different dietary conditions allows us to gain deeper insights into how specific nutrients and dietary factors affect the metabolic pathways and microbial functions within the cecum (Cai, Wen, Meng, & Yang, 2021) (Stanley, Geier, Chen, Hughes, & Moore, 2015). Recently, the metabolomic signatures and microbiome profiles of cecum contents in high-fat diet-induced obese mice have been investigated by UHPLC-Q-TOF/MS (Cai et al., 2021), 16S rRNA gene amplicon sequencing and gas chromatography–mass spectrometry (GC–MS) (Jo et al., 2021), and by ^{1}H NMR spectroscopy (Ogawa et al., 2020), recognizing that the comprehension of the effects of a high-fat diet *vs* a standard diet on cecal content is of paramount importance (Jo et al., 2021).

Here, we hypothesized that the investigation of the cecal content metabolic profile in mice fed a standard or high-fat diet can reflect

* Corresponding author.
E-mail address: beatrice.campanella@cnr.it (B. Campanella).

https://doi.org/10.1016/j.foodchem.2024.139856
Received 26 January 2024; Received in revised form 20 May 2024; Accepted 25 May 2024
Available online 28 May 2024

variations in the gut microbiota composition, providing a useful approach for understanding host-microbiome interactions and possible insights into the effects of dietary interventions.

FTIR is one of the spectroscopic methodological approaches widely employed in tandem with chemometric tools to evidence the differences between different groups of samples (control *vs* "treated" samples, control *vs* pathological samples…) (Ferreira et al., 2022; Magalhães, Goodfellow, & Nunes, 2021; Naseer, Ali, & Qazi, 2021; Talari, Martinez, Movasaghi, Rehman, & Rehman, 2017), like other spectroscopic approaches and chromatographic methods (LC or GC). FTIR spectroscopy is an excellent tool for profiling fecal extracts as it enables the simultaneous detection of various metabolites from a broad range of chemical classes, including short-chain fatty acids (SCFAs), amino acids, bile acids, carbohydrates, amines, and alcohols (Chakraborty & Das, 2017; Talari et al., 2017).

Few studies have been conducted on fecal samples (Ferreira et al., 2022; Franck, Sallerin, Schroeder, Gelot, & Nabet, 1996; Kho et al., 2023) using FTIR and even fewer on cecal content (Anderson et al., 2013; Daniel et al., 2014). FTIR spectroscopy has the advantage to be very rapid without requiring cumbersome sample preparation steps, especially performing the measurements with the "printing" method, as previously described by our group (Campanella, Legnaioli, Onor, Benedetti, & Bramanti, 2023).

This study aimed to investigate the water-soluble fraction of the cecal content of mice fed a high-fat diet *vs* a standard diet using ATR-FTIR spectroscopy, and to quantify the metabolite composition using liquid chromatography. To analyze the complex spectral dataset obtained from FTIR spectra, we employed Principal Component Analysis (PCA) (Morais, Lima, Singh, & Martin, 2020). FTIR spectroscopic analysis was sensitive enough to enable us to reveal distinct clustering patterns in the score plot, indicating significant variations in the metabolic profiles between the dietary groups. The implementation of FTIR study with liquid chromatography allowed us to obtain information on specific metabolites related to high-fat and standard diets responsible for the spectroscopic differences.

2. Materials and methods

2.1. In vivo animal experiment and dietary regimen

The *in vivo* experiment was conducted using male C57BL/6 J mice with a body weight range of 22–25 g. The mice were housed in cages under a 12 h light/dark cycle at room temperature, with relative humidity maintained at 55%. Throughout the experiment, both groups of mice had *ad libitum* access to food and drinking water.

The mice were randomly assigned to two groups: the control (standard diet, STD) group ($n = 12$) and the high-fat diet (HFD) group ($n = 11$; one mouse died before the end of the experiment). The randomization was performed using the simple randomization strategy by the online tool "Research Randomizer" (www.randomizer.org). The control group received a standard chow diet containing 19% proteins, 6% fibers, 7% minerals and vitamins moisture, 64% carbohydrates, and 4% fats, where the latter accounted for 11% of the diet-deriving energy. The high-fat diet group received a specialized diet (Research Diets, D12492) comprising 24% proteins, 6% fibers, 5% minerals and vitamins moisture, 26% carbohydrates, and 35% fats, with the 35% of fats contributing to 60% of the diet-deriving energy.

Ten weeks after the commencement of the trial, the mice were euthanized by cervical dislocation, and their cecal content was collected in sterilized conditions in a random order. The randomization was performed using the simple randomization strategy by "Research Randomizer" tool online (www.randomizer.org). The cecal contents were frozen in liquid nitrogen immediately after collection and stored in a freezer at −80 °C.

The animal procedures were carried out at the Centre of Experimental Biomedicine of CNR (Pisa, Italy) in accordance with the approved *in vivo* protocol (Protocol 65E5B.53) and authorized by the Italian Ministry of Health (Authorization 873/2021-PR of 12/11/21). All efforts were made to ensure the welfare and ethical treatment of the animals throughout the study.

2.2. Sample preparation

Approximately 45 mg of the cecal content samples were thawed and dissolved in 500 μL of bidistilled H_2O (ELGA Ultrapure Laboratory Water, Milan, Italy). The sample was homogenized by vortexing and sonication (40 kHz for 5 min). After sonication, the samples were centrifuged at 14000 rpm for 10 min. The supernatant was collected and stored in a freezer at −80 °C. For the analysis, the supernatant samples were thawed and split in two aliquots. The supernatants were fractionated in two parts: (i) a part was analyzed as is (named "untreated samples"); (ii) a part was deproteinized by ultracentrifugation (30 min) using Microcon® Centrifugal Filters with cut off 3-kDa (Merck, Milan Italy) (named "3-kDa filtered samples").(Campanella et al., 2023).

2.3. ATR-FTIR analysis

Five drops (50 μL each) of samples were deposited onto a polypropylene (PP) sheet by a micro-pipette (Eppendorf Research Plus pipette, Eppendorf AG), and air-dried at room temperature overnight. Spectra were recorded in ATR mode on sample dried spots using a Frontiers FTIR spectrometer (Perkin Elmer, Milan, Italy), equipped with a diamond attenuated total reflectance (ATR) sampling accessory. The flat sample press tip (2 mm diameter) was employed to "stamp" the sample from the dried spot (Fig. 1), then the PP sheet was removed. The micro-amount "printed" on the ATR diamond window was enough to get reliable and reproducible spectra, as previously reported (Fornasaro et al., 2022). Spectra were recorded in 4000–600 cm^{-1} spectral range with a 4 cm^{-1} resolution, with 32 scans for the background and the sample. For each analysis, the diamond sampling window and the sample press tip were cleaned with 70% ethanol v/v. Mid-infrared (MIR) spectra were acquired on 5 different spots for every mouse (12 + 11 independent samples) obtaining a CV% <3%, by far smaller than the biological variability. Fig. 1 schematizes the experimental procedure.

2.4. ATR-FTIR spectra preprocessing and analysis

Fig. S1 shows the original spectra obtained for both experiments (no cut-off and 3-kDa cut-off). Spectra pre-processing, analysis, and data visualization were performed within R environment - version 4.1.0 (2021–09-91) using the packages *hyperSpec*, *prcomp*, *stats*, *baseline* and *ggplot2*. An in-house modified R code from (Fornasaro et al., 2022) was used. The pre-processing steps were the following: (i) removal of the 1800–2800 cm^{-1} region, (ii) polynomial baseline subtraction (method "*modpolyfit*", degree = 4), (iii) vector normalization. Fig. S2 shows the spectra for both experiments (no cut-off and 3-kDa cut-off) after the described pretreatment. Before principal component analysis (PCA) spectra were mean centered. A Welch's *t*-test with Benjamini-Hochberg correction for false discovery rate was performed on PCA scores.

2.5. HPLC-DAD/FD analysis

3-kDa Filtered samples were 3-fold diluted in 5 mM sulfuric acid, filtered using a 0.20 μm RC Mini-Uniprep (Agilent Technologies, Milan, Italy) filter, injected in an Agilent 1260 Infinity HPLC system (Agilent Technologies, Milan, Italy) equipped with a UV/vis diode array (1260 DAD G4212B) and fluorescence (FD) detector ($V_{inj} = 5$ μL), and analyzed as described in the paper (Campanella et al., 2020). All reagents, having purity >99%, were purchased from Merck-Sigma (Merck, Milan, Italy) and used without previous purification.

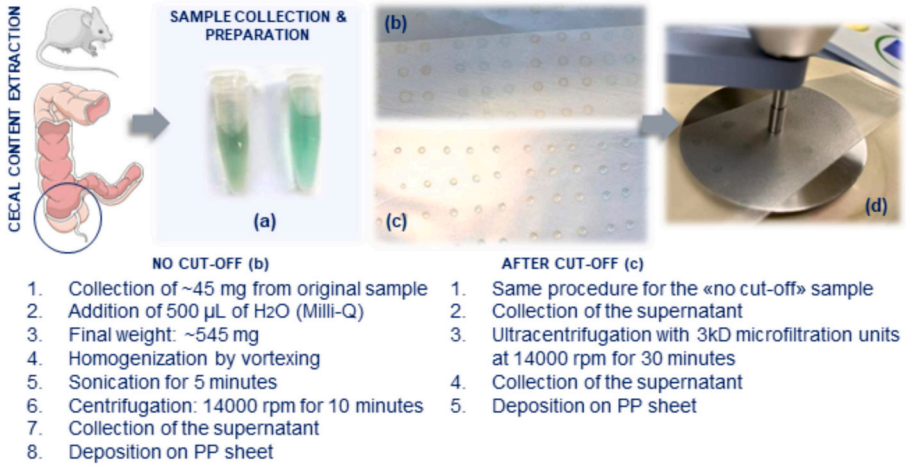

Fig. 1. Experimental procedure: workflow.

3. Results and discussion

3.1. FTIR spectral profiles of Cecal content

FTIR spectroscopy can be applied to analyze intestinal contents, and it provides valuable insights into the metabolic landscape of the gut microbiota. Fig. 2 shows the overlaid ATR-FTIR spectra of the untreated (Fig. 2A) and 3-kDa filtered cecum extracts (Fig. 2B) for the two groups fed the STD and HFD diet. These data were generated from all ATR-FTIR spectra of the entire dataset (120 spectra from untreated samples and 115 spectra from 3-kDa cut-off samples, Fig. S1) after the pre-treatment described in the Materials and Methods Section (Fig. S2). After spectral pre-treatment, the 3-kDa filtered samples appeared more homogeneous than the untreated samples.

Figs. 3 and 4 show the comparison between medians, generated by averaging the biological and instrumental replicas, and interquartile (shaded areas) of the ATR-FTIR spectra of STD (blue) and HFD (orange) groups, together with the median and interquartile of all the difference spectra (black) from the analysis of untreated samples (Fig. 3) and 3-kDa filtered samples (Fig. 4).

FTIR spectroscopic analysis of cecal content samples revealed distinct variations induced by different dietary regimens in both untreated and 3-kDa filtered samples. FTIR spectra of untreated samples have complex absorption bands in the O—H and N—H stretching region

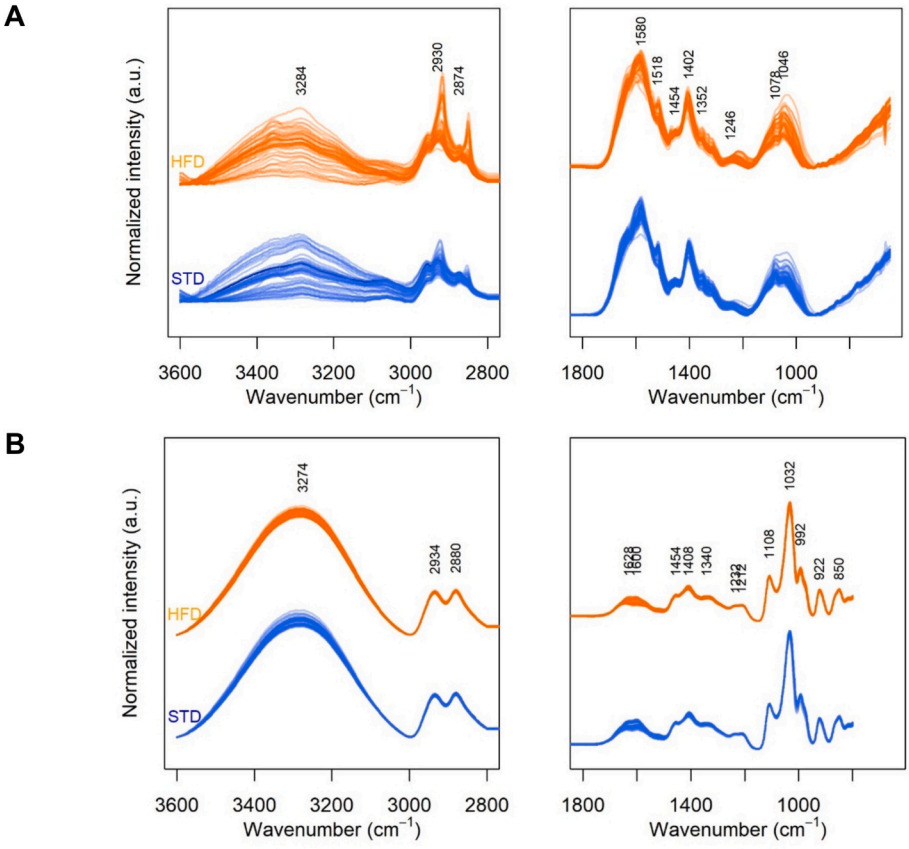

Fig. 2. Overlayed ATR-FTIR spectra of untreated (A panel) and 3-kDa filtered samples (B panel) for the 2 groups (STD: standard diet; HFD: high-fat diet).

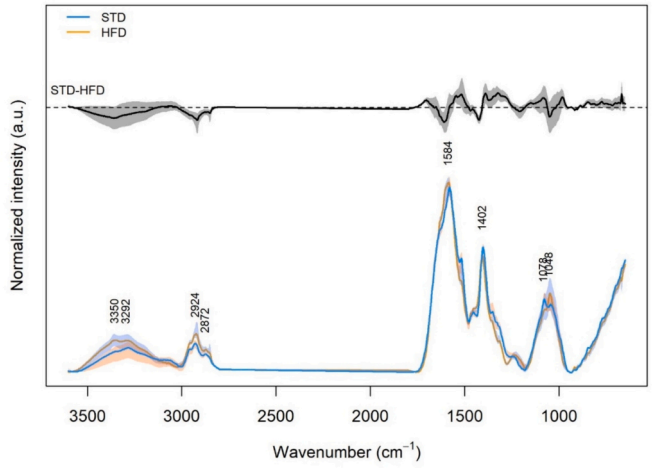

Fig. 3. Comparison between medians and interquartile (shaded areas) of the intensity for the ATR-FTIR spectra of standard (STD, blue) and high-fat diet (HFD, orange) groups, together with the median and interquartile of all the difference spectra (black) from the analysis of untreated samples. (For interpretation of the references to colour in this figure legend, the reader is referred to the web version of this article.)

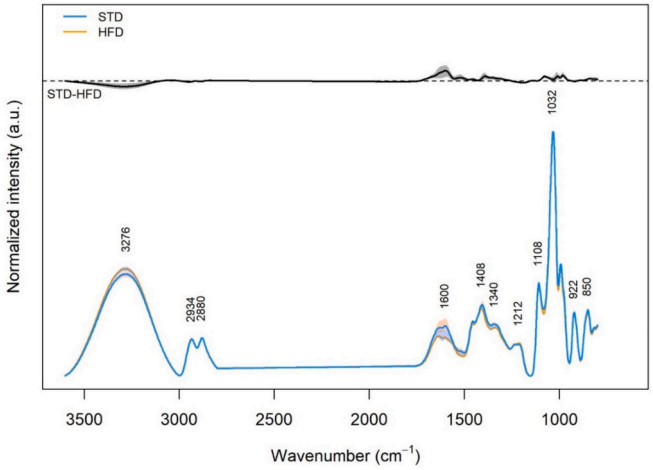

Fig. 4. Comparison between medians and interquartile (shaded areas) of the intensity for the ATR-FTIR spectra of standard (STD, blue) and high-fat diet (HFD, orange) groups, together with the median and interquartile of all the difference spectra (black) from the analysis of 3-kDa filtered samples. (For interpretation of the references to colour in this figure legend, the reader is referred to the web version of this article.)

(3800–3000 cm^{-1}), CH_2 and CH_3 stretching (2916 and 2850 cm^{-1}) and bending vibrations (1450, 1424 and 1362 cm^{-1}), C═O stretching, N–H bending and C–N stretching modes in the 1700–1500 cm^{-1} region typical of amines and amides, C—O (1208 cm^{-1}), C–O–C (1050 cm^{-1}) stretching, and C–O–H bending vibrations (1100–900 cm^{-1}). These bands can be due to polysaccharidic matrices (starch) (Anderson et al., 2013), starch bile derivates (Untereiner et al., 2014), amides (Daniel et al., 2014; Jameson, Olson, Kazmi, & Hsiao, 2020), proteins present in bile, and lipidic components (Untereiner et al., 2014). Despite the matrix complexity, we found that the diet impacts on these absorptions giving appreciable differences (Fig. 3 and Fig.S3A). The major differences observed in the spectra of untreated samples are due to the peaks at 3352, 2916, 2850, 1610, 1450, 1424, 1362, 1208, 1050, and 916 cm^{-1} characteristics of HFD (negative peaks) and 1544, 1514, 1388, 1322, 1078 and 980 cm^{-1} characteristic of STD (positive peaks) (Fig. S3A) (Daniel et al., 2014).

The analysis of 3-kDa filtered samples (Fig. 4) focus on the differences related to low-molecular-weight metabolites. Medians and interquartiles ATR-FTIR spectra of filtered samples have absorptions typical of glycerol and derivates, amides and derivates, amino acid side chains and short chain fatty acids (SCFAs) (https://sdbs.db.aist.go.jp/sdbs/cgi-bin/direct_frame_top.cgi, SDBS). After the 3-kDa filtration STD and HFD samples show differences (Fig. 4 and S3B), at 1594, 1514, 1448, 1386, 1346, 1074, 1008 and 980 cm^{-1} (positive peaks characteristics of STD) and at 3280, 2946, 2886 cm^{-1} (negative peaks characteristic of HFD) (Fig.S3B).

This first qualitative analysis suggests that FTIR analysis is a suitable, rapid tool for uncovering the impact of different dietary regimens on the gut's metabolic landscape.

3.2. Principal component analysis

To further explore the metabolic variations induced by different dietary regimens in mice, we performed Principal Component Analysis (PCA) on the FTIR spectral data of the cecal content samples. PCA analysis revealed distinct clustering patterns between the two dietary groups, indicating differences in the overall metabolite composition of the cecal content. The scores plot obtained from the PCA demonstrated a significant difference between the STD and HFD groups in both untreated and 3-kDa filtered samples, indicating that the dietary regimen strongly influences the cecal metabolite profile, according to the literature (Anderson et al., 2013; Cai et al., 2021; Daniel et al., 2014; Jo et al., 2021; Ryan, Barquera, Barata Cavalcanti, & Ralston, 2021; Van Treuren & Dodd, 2020; Zhang et al., 2023).

Fig. 5 shows PC1 vs PC3 and PC2 vs PC3 score plots from the PC analysis of untreated samples (panel A), the scores of the third principal component split by group (panel B), and PC3 loading (black lines) compared to corresponding ATR-FTIR average spectrum (blue line) (panel C).

In untreated samples, STD and HFD groups were separated along PC3. The *p*-value from STD-PC3 and HFD-PC3 comparison, obtained by a pairwise *t*-test (adjusted for false discovery rate with the Benjamini-Hochberg method) with no assumption of equal variances, was <0.001.

The analysis of the PC3 loading plot confirms the results of the analysis of median interquartile of the difference spectra. PC3 indicates that HFD affects IR absorptions typical of polysaccharidic matrices (starch) (Anderson et al., 2013), starch bile derivatives (Untereiner et al., 2014), amides (Daniel et al., 2014; Jameson et al., 2020), proteins present in bile, and lipidic components (Untereiner et al., 2014).

Fig. 6 shows PC1 vs PC3 and PC2 vs PC3 score plots from PC analysis of 3-kDa filtered samples (panel A), the scores of the first principal component split by group (panel B), and PC1 loading (black lines) from PC analysis compared to corresponding ATR-FTIR average spectrum (blue line) (panel C). The p-value, obtained from STD-PC1 *vs* HFD-PC1 comparison, was <0.001.

In the 3-kDa filtered samples, the STD and HFD groups were significantly separated along PC1 (Fig. 5). PC1 loadings indicate HFD group characterized by the absorption at 3298 cm^{-1}, typical of N—H stretching of secondary amide, and at 2958 and 2898 cm^{-1},typical of CH_2 and CH_3 stretching vibrations. The STD group is characterized by metabolites associated with the bands around 1602 and 1520 cm^{-1} attributed to amides and amines (Daniel et al., 2014; Jameson et al., 2020), and potentially to the asymmetric -COO− and the symmetric -COO− stretching of amino acid side chains, and to CH_2 and CH_3 bending vibrations, and peaks at 1082, 1012, 984 cm^{-1} characteristic of C—O and C-O-C compounds, including SCFAs, carbohydrates and glycerol/glycerol derivatives (Ogawa et al., 2020).

Despite the assignment of the absorption to specific low-molecular weight metabolites is not feasible using FTIR spectroscopy, and despite few authors report on the composition of mouse cecal content (Cai et al., 2021; Daniel et al., 2014; Ogawa et al., 2020; Sun et al., 2019; Zeng et al., 2015), by matching the available data several hypotheses on

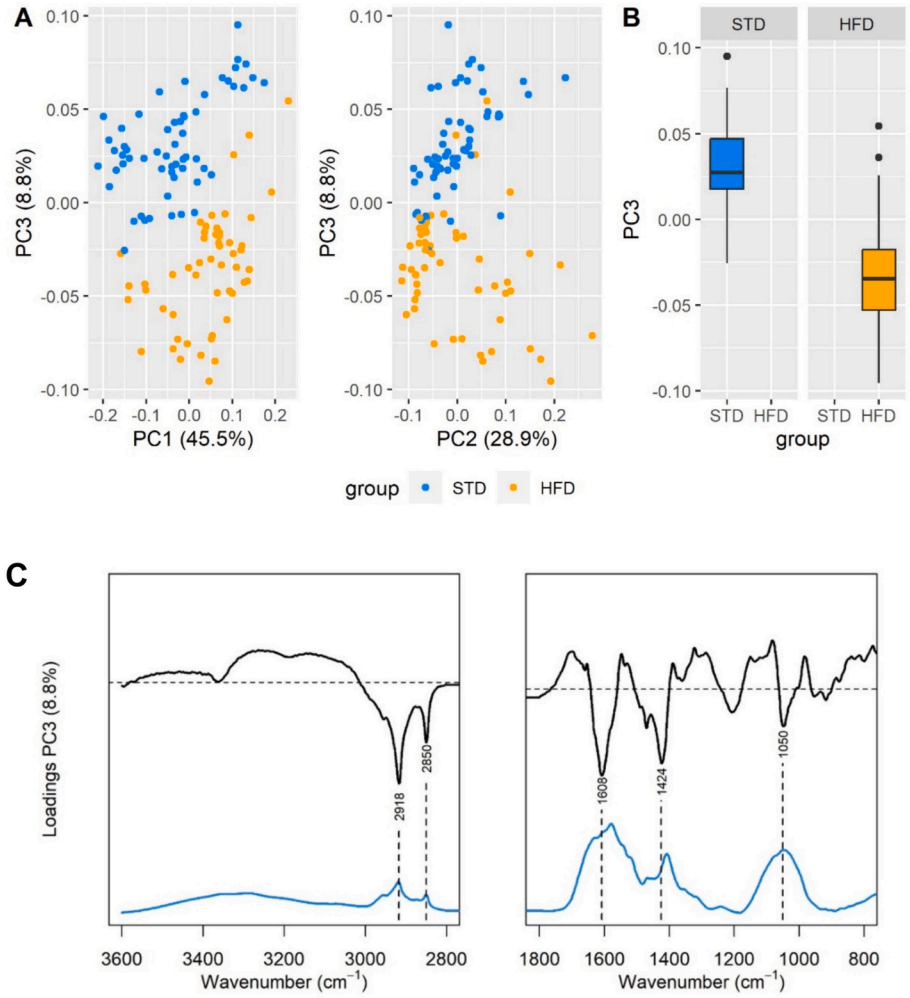

Fig. 5. (A) PC1 vs PC3 and PC2 vs PC3 score plots from PC analysis of untreated samples (A); (B) scores of the third principal component split by group (B). (C) PC3 loading (black lines) from PC analysis of untreated samples compared to the corresponding ATR-FTIR average spectrum (blue line). (For interpretation of the references to colour in this figure legend, the reader is referred to the web version of this article.)

the main molecules and pathways involved in the systemic effects of HFD can be suggested. Table S1 shows a list of metabolites, with the related concentration detected in mouse cecal content that could help in the interpretation of these differences, although the metabolite pattern may differ due to the adopted sample preparation methods.(Ogawa et al., 2020).

FTIR spectroscopic data have drawn attention to glycerol derivatives, amides, amino acids, and SCFAs. Although glycerol is among the most abundant compounds in mouse cecal content (Ogawa et al., 2020), its role remains unknown. It has been reported that human fecal microbiota displays variable patterns of glycerol metabolism, and that glycerol may modulate fermentation kinetics and profiles in the gastrointestinal tract, correlating with SCFA content (De Weirdt et al., 2010). It cannot be excluded that diet-modulated glycerol content and species are associated with 2-arachidonoyl glycerol metabolism, a molecule with cannabinoid neuromodulatory effects, and an inflammatory signaling role in the gut-brain axis (Wang, Su, Dai, Song, & Qian, 2023).

Regarding the detection of amide compounds in the cecal content of mice, it is interesting to highlight that N-acyl amides have emerged as a family of biologically active compounds in transient receptor potential channels, and conserved integral membrane proteins of ion channels (Raboune et al., 2014). N-acyl amides are characterized by an acyl group and an amine via an amide bond, and can be modified by changing either the fatty acid or the amide to potentially form hundreds of lipids representing the gut microbial lipidome (Morozumi, Ueda, Okahashi, & Arita, 2022). The involvement of SCFAs in the gut-brain signaling is also well known (Jameson et al., 2020; Wang et al., 2023).

3.3. HPLC-DAD/FD analysis of 3-kDa filtered cecal content samples

In our laboratories, we have developed a liquid chromatography method that exploits a diode array and a fluorescence detector for the quantification of low-molecular-weight metabolites in biological extracts. This procedure requires minimal sample handling and it is cost-effective, as it makes it possible to analyze a large number of samples with basic instrumentation. In this study, HPLC-DAD/FD analysis allowed us to add important pieces to the framework outlined by FTIR spectroscopy. Fig. 7 shows a box plot of 13 metabolites determined by HPLC-DAD/FD in the cecal content extracts of mice fed the two diets. Representative absorbance chromatograms at 220 nm of STD and HFD cecal content extracts are reported in the Supporting Information (Fig. S5).

The main metabolites in the millimolar range are the SCFAs acetic, propionic, succinic, formic and malic acids. In the micromolar range, isobutyric and butyric acids, pyridoxine (vitamin B6), uric acid, and aromatic amino acids phenylalanine (PHE), tyrosine (TYR), and tryptophan (TRP), were detected. Significant differences were observed in

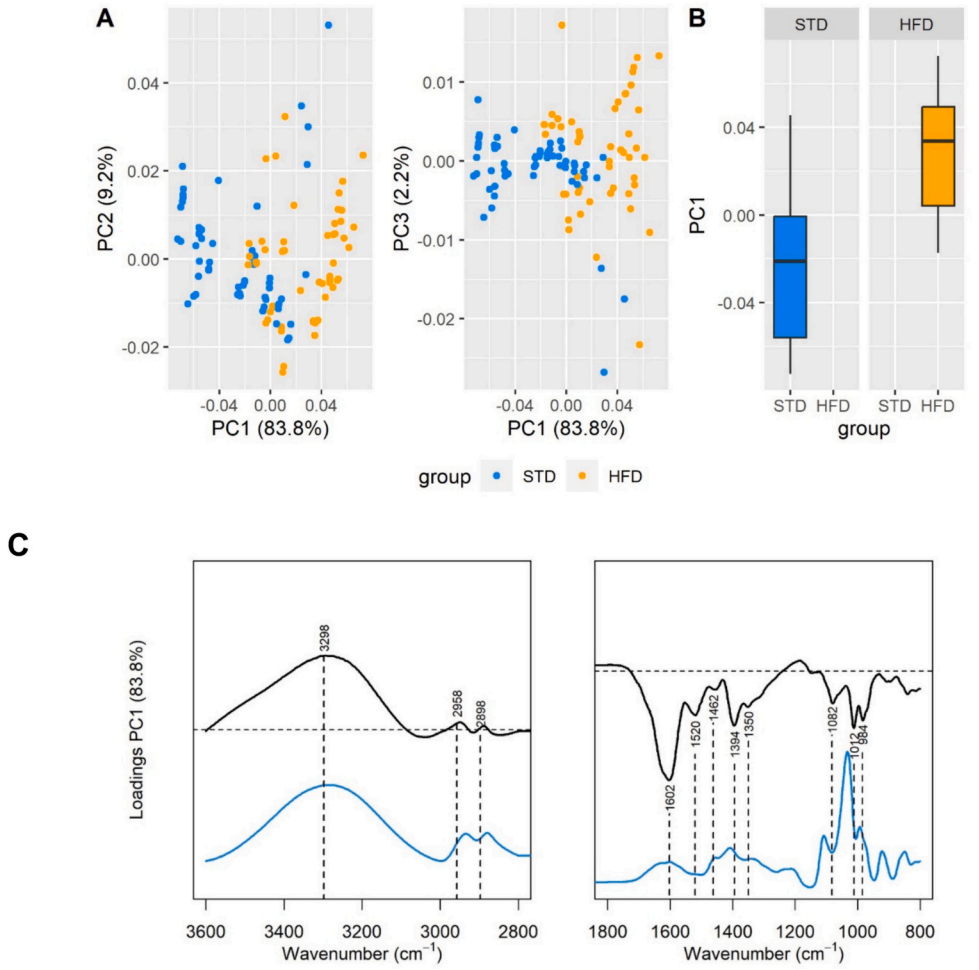

Fig. 6. PC1 vs PC2 and PC1 vs PC3 score plots from PC analysis of 3 kDa filtered samples (A); (B) scores of the first principal component split by group (B). (C) PC1 loading (black lines) from PC analysis of 3-kDa filtered samples compared to corresponding ATR-FTIR average spectrum (blue line). (For interpretation of the references to colour in this figure legend, the reader is referred to the web version of this article.)

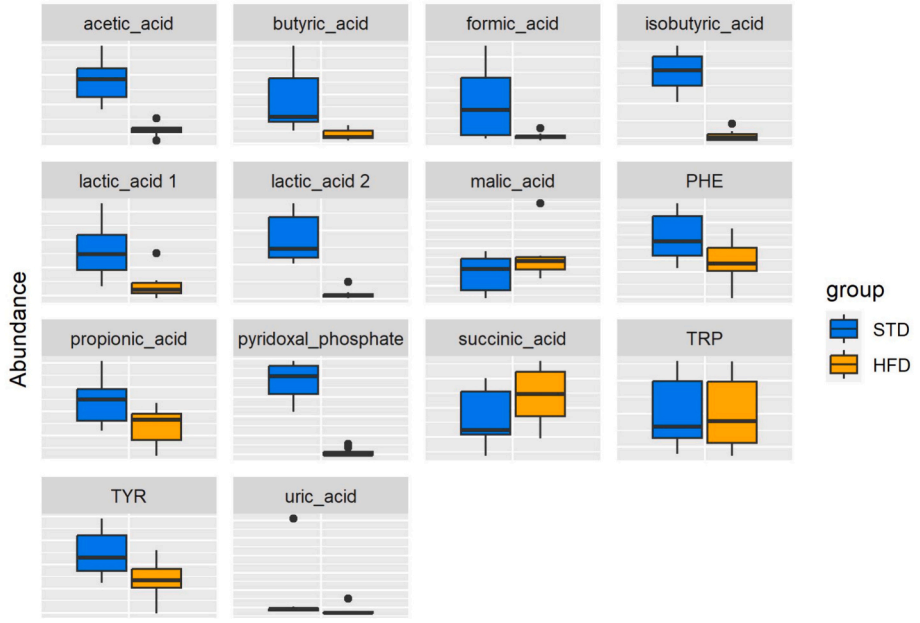

Fig. 7. Box plot of metabolites (autoscaled concentrations) determined by HPLC-DAD in the cecal content extracts of $N = 11$ animal fed with standard and high-fat diet.

10 out of 13 (*t*-test comparison) of the listed metabolites, partially explaining the differences observed in the FTIR analysis. Table 1 shows the descriptive statistics of the 13 metabolites in the cecal content extracts determined by HPLC-DAD (μmol/g cecal content).

Acetate is a crucial SCFA present in the gut, especially in the colon, with trophic effects on the colonic epithelium and mucosal blood flux (Vernocchi, Del Chierico, & Putignani, 2016), and the knowledge of the role of microbiota-derived acetate in health and disease is increasing (Antunes et al., 2019; Bhattarai et al., 2017; Chen et al., 2023; Erny et al., 2021; Jugder, Kamareddine, & Watnick, 2021; Lin et al., 2022; Marques et al., 2017; Niu et al., 2023; Zhang et al., 2023). The other SCFAs, propionate (Bai et al., 2021; Bajic et al., 2020; Bindels et al., 2012; Chen et al., 2021; Dürholz et al., 2022; Hou et al., 2021; Huang et al., 2020; Huang, Shi, Xu, & Ji, 2021; Kim et al., 2019; Langfeld, Du, Bereswill, & Heimesaat, 2021; Li et al., 2021; Su, Braat, & Peppelenbosch, 2021; Yan et al., 2022) and butyrate (Amiri et al., 2022; Bridgeman et al., 2020; Couto, Gonçalves, Magro, & Martel, 2020; Gheorghe et al., 2022; Stilling et al., 2016) are involved as well in important metabolic pathways and systemic conditions. All SCFA concentrations were decreased in the HFD group.

Lactate is a common metabolite in mammals, human body, and biofluids, and plays a role in the glycolysis-oxidative metabolism switch (Brooks, 2018). However, its role in gut remains unclear and under study (Lee et al., 2018; Mayeur et al., 2013; Okada et al., 2013; Peng, & TH, D., & Zhang, M., 2016; Zhao, Dong, Zhang, & Li, 2019). In our experiment, mice fed an HFD had significantly lower lactate levels.

Gut bacteria are also involved in the biosynthesis of B-vitamins B1 (thiamin), B2 (riboflavin), B3 (niacin), B5 (pantothenic acid), B6 (pyridoxine), B7 (biotin), B9 (folate), and B12 (cobalamin), which are involved in a variety of metabolic pathways and physiopathological conditions (Barone, D'Amico, Brigidi, & Turroni, 2022; Magnúsdóttir, Ravcheev, de Crécy-Lagard, & Thiele, 2015; Miri, Yeo, Abubaker, & Hammami, 2023; Thakur, Tomar, & De, 2016). HFD samples showed significant lower concentrations of vitamin B6, which is the cofactor of pyridoxal phosphate-dependent (B6-dependent) enzymes and in methionine and transsulfuration pathways that convert homocysteine to cysteine (Ettinger, 2022).

The decrease of aromatic amino acids in cecal content of HFD mice was less evident for TYR and PHE, or absent for TRP. However, the fluorescence detector provided evidence of relevant changes in the chromatograms (λ_{ex} = 280 nm, λ_{em} = 320 nm) of STD and HFD mice. Fig. 8 shows the comparison of the average fluorescence chromatograms of STD and HFD samples (N = 15 samples considering biological and instrumental replicates, metadata are available). Fig. S5 shows the fluorescence chromatograms of standard solutions of 10 μM dopamine, 2.34 μM TYR, 45.1 μM PHE, 8.97 μM TRP and 2 μM melatonin.

The results revealed different peaks in the STD and HFD groups. Among these, only the peaks at 7.819 and 23.508 min were identified as TYR and TRP, respectively. Dopamine and melatonin were eluted at 5.328 and 27.023 min, respectively. However, many peaks in the fluorescence chromatograms (λ_{ex} = 280 nm/ λ_{em} = 320 nm) were not identified. Considering that TYR is crucial for the production of dopamine and TRP to produce serotonin and melatonin, and that TRP metabolites are strictly related to the gut-brain axis (Gao & Farzi, 2020), TRP/TYR metabolites and small TRP/TYR-containing peptides would require further investigation.

4. Conclusions

FTIR spectroscopic and chromatographic data suggest that dietary variations affect the high- and low- molecular-weight metabolite profiles of cecal content extracts. The FTIR method with the deposition of the extracts on polypropylene sheets has provided a valuable, fast tool for the efficient, low-cost, and reliable characterization of cecal content metabolites, demonstrating the potentiality of the ATR-FTIR method for studying the impact of diet on gut content composition and identifying regions of the spectra associated with potential biomarkers correlated with the diet. Complementary liquid chromatography allowed us to identify several metabolites and elucidate their variations among the different diet groups, being SCFAs, lactate and aromatic amino acids the main low-molecular-weight compounds involved in differentiating STD from HFD.

These data confirm the complex metabolic interactions between the gut microbiota, host factors, and dietary components in mice. Alterations in their intensities or patterns suggest metabolic adaptations in response to a high-fat diet.

The ability to analyze multiple metabolites simultaneously makes the FTIR approach rapidly and non-destructively well suited for high-throughput investigations and may facilitate the development of targeted interventions in animal models to improve gut health and manage diet-related diseases.

CRediT authorship contribution statement

Cheherazade Trouki: Writing – original draft, Investigation, Formal analysis. **Beatrice Campanella:** Writing – review & editing, Visualization, Validation, Formal analysis. **Massimo Onor:** Formal analysis. **Andrea Vornoli:** Writing – review & editing, Methodology. **Luisa Pozzo:** Writing – review & editing, Methodology, Conceptualization. **Vincenzo Longo:** Writing – review & editing, Methodology,

Table 1
Descriptive statistics of the 13 metabolites in the cecal content extracts determined by HPLC-DAD (μmol/g cecal content).

	STANDARD DIET													
	formic acid	malic acid	lactic acid 1	lactic acid 2	acetic acid	uric acid	pyridoxal phosphate	succinic acid	TYR	propionic acid	PHE	isobutyric acid	butyric acid	TRP
Min.	1.3	2.6	26.4	83.3	188.7	0.06	1.0	34.8	0.56	86.5	2.4	7.6	2.6	0.44
1st Qu.	3.6	6.6	50.8	96.6	260.2	0.10	1.4	54.2	0.78	120.5	3.3	10.8	4.0	0.57
Median	22.2	17.6	74.0	116.3	360.7	0.15	1.8	58.2	1.0	192.5	4.4	13.8	4.9	0.66
Mean	28.4	15.3	80.6	142.9	356.9	0.34	1.7	69.3	1.1	192.6	4.7	13.3	6.9	0.78
3rd Qu.	45.6	22.9	102.1	185.7	424.0	0.17	2.0	93.7	1.4	229.4	6.2	16.5	11.1	1.0
Max.	68.9	26.7	148.8	216.3	554.5	3.2	2.1	106.2	1.7	326.0	7.1	18.7	16.4	1.2
	HIGH-FAT DIET													
	formic acid	malic acid	lactic acid 1	lactic acid 2	acetic acid	uric acid	pyridoxal phosphate	succinic acid	TYR	propionic acid	PHE	isobutyric acid	butyric acid	TRP
Min.	0.00	12.8	9.3	7.8	11.6	0.00	0.08	50.7	0.01	0.00	0.24	0.00	1.0	0.42
1st Qu.	1.8	17.4	16.4	10.3	58.4	0.01	0.09	70.9	0.47	53.3	2.2	0.02	1.4	0.53
Median	2.4	21.5	21.3	12.5	67.2	0.02	0.10	91.5	0.60	123.4	2.7	0.55	1.6	0.70
Mean	2.7	22.0	25.6	15.1	66.7	0.06	0.13	89.2	0.66	108.9	3.1	0.81	1.9	0.75
3rd Qu.	3.6	23.6	31.7	15.7	84.3	0.04	0.15	111.9	0.80	144.6	3.9	1.2	2.6	1.0
Max.	8.9	51.5	75.1	43.5	138.8	0.50	0.32	122.0	1.1	180.6	5.3	3.3	3.5	1.2

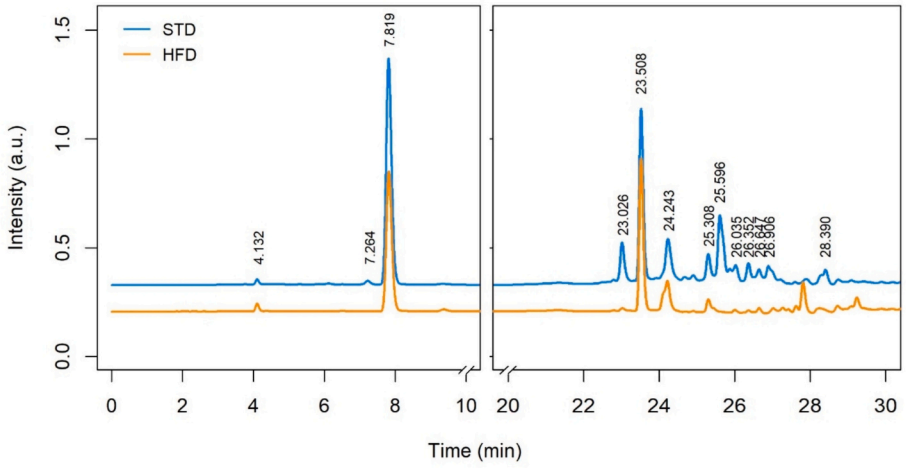

Fig. 8. Fluorescence chromatogram of STD (blue line) and HFD (orange line) samples. (For interpretation of the references to colour in this figure legend, the reader is referred to the web version of this article.)

Conceptualization. **Emilia Bramanti:** Writing – original draft, Supervision, Methodology, Conceptualization.

Declaration of competing interest

The authors declare that they have no known competing financial interests or personal relationships that could have appeared to influence the work reported in this paper.

Data availability

Data will be made available on request.

Appendix A. Supplementary data

Supplementary data to this article can be found online at https://doi.org/10.1016/j.foodchem.2024.139856.

References

Amiri, P., Hosseini, S. A., Ghaffari, S., Tutunchi, H., Ghaffari, S., Mosharkesh, E., & Roshanravan, N. (2022). Role of butyrate, a gut microbiota derived metabolite, in cardiovascular diseases: A comprehensive narrative review. *Frontiers in Pharmacology, 12*, Article 837509.

Anderson, T. J., Ai, Y., Jones, R. W., Houk, R. S., Jane, J.-l., Zhao, Y., . . . McClelland, J. F. (2013). Analysis of resistant starches in rat cecal contents using Fourier transform infrared photoacoustic spectroscopy. Journal of Agricultural and Food Chemistry, 61 (8), 1818–1822.

Antunes, K. H., Fachi, J. L., de Paula, R., da Silva, E. F., Pral, L. P., Dos Santos, A.Á., & Mayer, F. Q. (2019). Microbiota-derived acetate protects against respiratory syncytial virus infection through a GPR43-type 1 interferon response. *Nature Communications, 10*(1), 3273.

Bai, Y., Li, Y., Marion, T., Tong, Y., Zaiss, M. M., Tang, Z., & Luo, Y. (2021). Resistant starch intake alleviates collagen-induced arthritis in mice by modulating gut microbiota and promoting concomitant propionate production. *Journal of Autoimmunity, 116*, Article 102564.

Bajic, D., Niemann, A., Hillmer, A.-K., Mejias-Luque, R., Bluemel, S., Docampo, M., & Schnabl, B. (2020). Gut microbiota-derived propionate regulates the expression of Reg3 mucosal lectins and ameliorates experimental colitis in mice. *Journal of Crohn's and Colitis, 14*(10), 1462–1472.

Barone, M., D'Amico, F., Brigidi, P., & Turroni, S. (2022). Gut microbiome–micronutrient interaction: The key to controlling the bioavailability of minerals and vitamins? *Biofactors, 48*(2), 307–314.

Bhattarai, Y., Schmidt, B. A., Linden, D. R., Larson, E. D., Grover, M., Beyder, A., & Kashyap, P. C. (2017). Human-derived gut microbiota modulates colonic secretion in mice by regulating 5-HT3 receptor expression via acetate production. *American journal of physiology-Gastrointestinal and liver physiology, 313*(1), G80–G87.

Bindels, L. B., Porporato, P., Dewulf, E., Verrax, J., Neyrinck, A. M., Martin, J., & Muccioli, G. (2012). Gut microbiota-derived propionate reduces cancer cell proliferation in the liver. *British Journal of Cancer, 107*(8), 1337–1344.

Breton, J., Galmiche, M., & Déchelotte, P. (2022). Dysbiotic gut bacteria in obesity: An overview of the metabolic mechanisms and therapeutic perspectives of next-generation probiotics. *Microorganisms, 10*(2), 452.

Breves, G. (1995). Short-chain fatty acid in the hindgut. *Physiological and clinical aspect of short-chain fatty acids*, 73–86.

Bridgeman, S. C., Northrop, W., Melton, P. E., Ellison, G. C., Newsholme, P., & Mamotte, C. D. (2020). Butyrate generated by gut microbiota and its therapeutic role in metabolic syndrome. *Pharmacological Research, 160*, Article 105174.

Brooks, G. A. (2018). The science and translation of lactate shuttle theory. *Cell Metabolism, 27*(4), 757–785.

Cai, H., Wen, Z., Meng, K., & Yang, P. (2021). Metabolomic signatures for liver tissue and cecum contents in high-fat diet-induced obese mice based on UHPLC-Q-TOF/MS. *Nutrition & Metabolism, 18*(1), 69.

Campanella, B., Legnaioli, S., Onor, M., Benedetti, E., & Bramanti, E. (2023). The role of the Preanalytical step for human saliva analysis via vibrational spectroscopy. *Metabolites, 13*(3), 393.

Campanella, B., Lomonaco, T., Benedetti, E., Onor, M., Nieri, R., & Bramanti, E. (2020). Validation and application of a derivatization-free RP-HPLC-DAD method for the determination of low molecular weight salivary metabolites. *International Journal of Environmental Research and Public Health, 17*(17), 6158.

Chakraborty, J., & Das, S. (2017). Application of spectroscopic techniques for monitoring microbial diversity and bioremediation. *Applied Spectroscopy Reviews, 52*(1), 1–38.

Chen, L., Zhou, X., Wang, Y., Wang, D., Ke, Y., & Zeng, X. (2021). Propionate and butyrate produced by gut microbiota after probiotic supplementation attenuate lung metastasis of melanoma cells in mice. *Molecular Nutrition & Food Research, 65*(15), 2100096.

Chen, M., Peng, L., Zhang, C., Liu, Q., Long, T., & Xie, Q. (2023). Gut microbiota might mediate the benefits of high-fiber/acetate diet to cardiac hypertrophy mice. *Journal of Physiology and Biochemistry, 79*(4), 745–756.

Couto, M. R., Gonçalves, P., Magro, F., & Martel, F. (2020). Microbiota-derived butyrate regulates intestinal inflammation: Focus on inflammatory bowel disease. *Pharmacological Research, 159*, Article 104947.

Daniel, H., Gholami, A. M., Berry, D., Desmarchelier, C., Hahne, H., Loh, G., & Walker, A. (2014). High-fat diet alters gut microbiota physiology in mice. *The ISME Journal, 8* (2), 295–308.

De Weirdt, R., Possemiers, S., Vermeulen, G., Moerdijk-Poortvliet, T. C., Boschker, H. T., Verstraete, W., & Van de Wiele, T. (2010). Human faecal microbiota display variable patterns of glycerol metabolism. *FEMS Microbiology Ecology, 74*(3), 601–611.

Dürholz, K., Schmid, E., Frech, M., Azizov, V., Otterbein, N., Lucas, S., & Zaiss, M. M. (2022). Microbiota-derived propionate modulates megakaryopoiesis and platelet function. *Frontiers in Immunology, 13*, Article 908174.

Erny, D., Dokalis, N., Mezö, C., Castoldi, A., Mossad, O., Staszewski, O., & Mayer, A. (2021). Microbiota-derived acetate enables the metabolic fitness of the brain innate immune system during health and disease. *Cell Metabolism, 33*(11), 2260–2276 (e2267).

Ettinger, S. (2022). Diet, gut microbiome, and cognitive decline. *Current Nutrition Reports, 11*(4), 643–652.

Ferreira, L., Machado, N., Gouvinhas, I., Santos, S., Celaya, R., Rodrigues, M., & Barros, A. (2022). Application of Fourier transform infrared spectroscopy (FTIR) techniques in the mid-IR (MIR) and near-IR (NIR) spectroscopy to determine n-alkane and long-chain alcohol contents in plant species and faecal samples. *Spectrochimica Acta Part A: Molecular and Biomolecular Spectroscopy, 280*, Article 121544.

Flint, H. J., Scott, K. P., Louis, P., & Duncan, S. H. (2012). The role of the gut microbiota in nutrition and health. *Nature Reviews Gastroenterology & Hepatology, 9*(10), 577–589.

Fornasaro, S., Esposito, A., Florian, F., Pallavicini, A., De Leo, L., Not, T., & Sergo, V. (2022). Spectroscopic investigation of faeces with surface-enhanced Raman scattering: A case study with coeliac patients on gluten-free diet. *Analytical and Bioanalytical Chemistry, 414*(11), 3517–3527.

Franck, P., Sallerin, J., Schroeder, H., Gelot, M., & Nabet, P. (1996). Rapid determination of fecal fat by Fourier transform infrared analysis (FTIR) with partial least-squares

regression and an attenuated total reflectance accessory. *Clinical Chemistry, 42*(12), 2015–2020.
Gao, K., Mu, C.-l., Farzi, A., & Zhu, W.-y. (2020). Tryptophan metabolism: A link between the gut microbiota and brain. Advances in Nutrition, 11(3), 709–723.
Gheorghe, A. S., Negru, Ș. M., Preda, M., Mihăilă, R. I., Komporaly, I. A., Dumitrescu, E. A., & Radu, E. A. (2022). Biochemical and metabolical pathways associated with microbiota-derived butyrate in colorectal cancer and omega-3 fatty acids implications: A narrative review. *Nutrients, 14*(6), 1152.
Hou, Y.-F., Shan, C., Zhuang, S.-Y., Zhuang, Q.-Q., Ghosh, A., Zhu, K.-C., . . . Yang, Y.-Y. (2021). Gut microbiota-derived propionate mediates the neuroprotective effect of osteocalcin in a mouse model of Parkinson's disease. Microbiome, 9, 1–17.
Huang, J.-F., Zhao, Q., Dai, M.-Y., Xiao, X.-R., Zhang, T., Zhu, W.-F., & Li, F. (2020). Gut microbiota protects from triptolide-induced hepatotoxicity: Key role of propionate and its downstream signalling events. *Pharmacological Research, 155*, Article 104752.
Huang, T., Shi, H., Xu, Y., & Ji, L. (2021). The gut microbiota metabolite propionate ameliorates intestinal epithelial barrier dysfunction-mediated Parkinson's disease via the AKT signaling pathway. *Neuroreport, 32*(3), 244–251.
Jameson, K. G., Olson, C. A., Kazmi, S. A., & Hsiao, E. Y. (2020). Toward understanding microbiome-neuronal signaling. *Molecular Cell, 78*(4), 577–583.
Jandhyala, S. M., Talukdar, R., Subramanyam, C., Vuyyuru, H., Sasikala, M., & Reddy, D. N. (2015). Role of the normal gut microbiota. *World Journal of Gastroenterology: WJG, 21*(29), 8787.
Jo, J.-K., Seo, S.-H., Park, S.-E., Kim, H.-W., Kim, E.-J., Kim, J.-S., & Park, D.-H. (2021). Gut microbiome and metabolome profiles associated with high-fat diet in mice. *Metabolites, 11*(8), 482.
Jugder, B.-E., Kamareddine, L., & Watnick, P. I. (2021). Microbiota-derived acetate activates intestinal innate immunity via the Tip60 histone acetyltransferase complex. *Immunity, 54*(8), 1683–1697 (e1683).
Kho, E. A., Fernandes, J. N., Tilbrook, A. J., Fox, G. P., Sikulu-Lord, M. T., Kotze, A. C., & Cozzolino, D. (2023). State of the art and the future of fecal analysis using infrared spectroscopy. *Applied Spectroscopy Reviews, 58*(10), 755–785.
Kim, K., Kwon, O., Ryu, T. Y., Jung, C. R., Kim, J., Min, J. K., & Cho, H. S. (2019). Propionate of a microbiota metabolite induces cell apoptosis and cell cycle arrest in lung cancer. *Molecular Medicine Reports, 20*(2), 1569–1574.
Langfeld, L. Q., Du, K., Bereswill, S., & Heimesaat, M. M. (2021). A review of the antimicrobial and immune-modulatory properties of the gut microbiota-derived short chain fatty acid propionate–what is new? *European Journal of Microbiology and Immunology, 11*(2), 50–56.
Lee, Y.-S., Kim, T.-Y., Kim, Y., Lee, S.-H., Kim, S., Kang, S. W., & Park, Y.-Y. (2018). Microbiota-derived lactate accelerates intestinal stem-cell-mediated epithelial development. *Cell Host & Microbe, 24*(6), 833–846 (e836).
Li, H., Zhao, L., Liu, S., Zhang, Z., Wang, X., & Lin, H. (2021). Propionate inhibits fat deposition via affecting feed intake and modulating gut microbiota in broilers. *Poultry Science, 100*(1), 235–245.
Lin, C.-J., Cheng, Y.-C., Chen, H.-C., Chao, Y.-K., Nicholson, M. W., Yen, E. C., & Hsieh, P. C. (2022). Commensal gut microbiota-derived acetate and propionate enhance heart adaptation in response to cardiac pressure overload in mice. *Theranostics, 12*(17), 7319.
Magalhães, S., Goodfellow, B. J., & Nunes, A. (2021). FTIR spectroscopy in biomedical research: How to get the most out of its potential. *Applied Spectroscopy Reviews, 56*(8–10), 869–907.
Magnúsdóttir, S., Ravcheev, D., de Crécy-Lagard, V., & Thiele, I. (2015). Systematic genome assessment of B-vitamin biosynthesis suggests co-operation among gut microbes. *Frontiers in Genetics, 6*, Article 129714.
Marques, F. Z., Nelson, E., Chu, P.-Y., Horlock, D., Fiedler, A., Ziemann, M., & El-Osta, A. (2017). High-fiber diet and acetate supplementation change the gut microbiota and prevent the development of hypertension and heart failure in hypertensive mice. *Circulation, 135*(10), 964–977.
Mayeur, C., Gratadoux, J.-J., Bridonneau, C., Chegdani, F., Larroque, B., Kapel, N., & Joly, F. (2013). Faecal D/L lactate ratio is a metabolic signature of microbiota imbalance in patients with short bowel syndrome. *PLoS One, 8*(1), Article e54335.
Miri, S., Yeo, J., Abubaker, S., & Hammami, R. (2023). Neuromicrobiology, an emerging neurometabolic facet of the gut microbiome? *Frontiers in Microbiology, 14*, 1098412.
Morais, C. L., Lima, K. M., Singh, M., & Martin, F. L. (2020). Tutorial: multivariate classification for vibrational spectroscopy in biological samples. *Nature Protocols, 15*(7), 2143–2162.
Morozumi, S., Ueda, M., Okahashi, N., & Arita, M. (2022). Structures and functions of the gut microbial lipidome. *Biochimica et Biophysica Acta (BBA)-molecular and cell biology of. Lipids, 1867*(3), Article 159110.
Naseer, K., Ali, S., & Qazi, J. (2021). ATR-FTIR spectroscopy as the future of diagnostics: A systematic review of the approach using bio-fluids. *Applied Spectroscopy Reviews, 56*(2), 85–97.
Nguyen, T. L. A., Vieira-Silva, S., Liston, A., & Raes, J. (2015). How informative is the mouse for human gut microbiota research? *Disease Models & Mechanisms, 8*(1), 1–16.
Niu, J., Cui, M., Yang, X., Li, J., Yao, Y., Guo, Q., & Zhang, C. (2023). Microbiota-derived acetate enhances host antiviral response via NLRP3. *Nature Communications, 14*(1), 642.
Ogawa, Y., Miyoshi, C., Obana, N., Yajima, K., Hotta-Hirashima, N., Ikkyu, A., & Yanagisawa, M. (2020). Gut microbiota depletion by chronic antibiotic treatment alters the sleep/wake architecture and sleep EEG power spectra in mice. *Scientific Reports, 10*(1), 19554.
Okada, T., Fukuda, S., Hase, K., Nishiumi, S., Izumi, Y., Yoshida, M., & Oshio, T. (2013). Microbiota-derived lactate accelerates colon epithelial cell turnover in starvation-refed mice. *Nature Communications, 4*(1), 1654.
Peng, S., & TH, D., & Zhang, M.. (2016). Changes in gut microbiota and serum D-lactate level and correlation analysis in children with recurrent pneumonia. *Zhongguo dang dai er ke za zhi= Chinese journal of. Contemporary Pediatrics, 18*(2), 113–116.
Raboune, S., Stuart, J. M., Leishman, E., Takacs, S. M., Rhodes, B., Basnet, A., & Bradshaw, H. B. (2014). Novel endogenous N-acyl amides activate TRPV1-4 receptors, BV-2 microglia, and are regulated in brain in an acute model of inflammation. *Frontiers in Cellular Neuroscience, 8*, 195.
Ryan, D., Barquera, S., Barata Cavalcanti, O., & Ralston, J. (2021). The global pandemic of overweight and obesity: Addressing a twenty-first century multifactorial disease. In *Handbook of global health* (pp. 739–773). Springer.
Stanley, D., Geier, M. S., Chen, H., Hughes, R. J., & Moore, R. J. (2015). Comparison of fecal and cecal microbiotas reveals qualitative similarities but quantitative differences. *BMC Microbiology, 15*, 1–11.
Stilling, R. M., Van De Wouw, M., Clarke, G., Stanton, C., Dinan, T. G., & Cryan, J. F. (2016). The neuropharmacology of butyrate: The bread and butter of the microbiota-gut-brain axis? *Neurochemistry International, 99*, 110–132.
Su, J., Braat, H., & Peppelenbosch, M. P. (2021). Gut microbiota-derived propionate production may explain beneficial effects of intermittent fasting in experimental colitis. *Journal of Crohn's and Colitis, 15*(6), 1081–1082.
Sun, L., Jia, H., Li, J., Yu, M., Yang, Y., Tian, D., & Zou, Z. (2019). Cecal gut microbiota and metabolites might contribute to the severity of acute myocardial ischemia by impacting the intestinal permeability, oxidative stress, and energy metabolism. *Frontiers in Microbiology, 10*, 1745.
Talari, A. C. S., Martinez, M. A. G., Movasaghi, Z., Rehman, S., & Rehman, I. U. (2017). Advances in Fourier transform infrared (FTIR) spectroscopy of biological tissues. *Applied Spectroscopy Reviews, 52*(5), 456–506.
Thakur, K., Tomar, S. K., & De, S. (2016). Lactic acid bacteria as a cell factory for riboflavin production. *Microbial Biotechnology, 9*(4), 441–451.
Untereiner, V., Dhruvananda Sockalingum, G., Garnotel, R., Gobinet, C., Ramaholimihaso, F., Ehrhard, F., & Thiéfin, G. (2014). Bile analysis using high-throughput FTIR spectroscopy for the diagnosis of malignant biliary strictures: A pilot study in 57 patients. *Journal of Biophotonics, 7*(3–4), 241–253.
Van Treuren, W., & Dodd, D. (2020). Microbial contribution to the human metabolome: Implications for health and disease. *Annual Review of Pathology: Mechanisms of Disease, 15*, 345–369.
Vernocchi, P., Del Chierico, F., & Putignani, L. (2016). Gut microbiota profiling: Metabolomics based approach to unravel compounds affecting human health. *Frontiers in Microbiology, 7*, Article 186329.
Wang, C.-Q., Su, Z., Dai, C.-G., Song, J.-L., & Qian, B. (2023). Multi-omics analysis reveals BDE47 induces depression-like behaviors in mice by interfering with the 2-arachidonoyl glycerol-associated microbiota-gut-brain axis. *Ecotoxicology and Environmental Safety, 259*, Article 115041.
Yan, J., Pan, Y., Shao, W., Wang, C., Wang, R., He, Y., & Wang, Z. (2022). Beneficial effect of the short-chain fatty acid propionate on vascular calcification through intestinal microbiota remodelling. *Microbiome, 10*(1), 195.
Zeng, H., Grapov, D., Jackson, M. I., Fahrmann, J., Fiehn, O., & Combs, G. F., Jr. (2015). Integrating multiple analytical datasets to compare metabolite profiles of mouse colonic-cecal contents and feces. *Metabolites, 5*(3), 489–501.
Zhang, Q., Cheng, J., Jiang, X., Tang, J., Zhu, C., Chen, H., & Laghi, L. (2023). Metabolomic characteristics of cecum contents in high-fat-diet-induced obese mice intervened with different fibers. *Foods, 12*(7), 1403.
Zhang, Q., Meng, N., Liu, Y., Zhao, H., Zhao, Z., Hao, D., & Ma, J. (2023). Protection effect of gut microbiota composition and acetate absorption against hypertension-induced damages on the longevity population in Guangxi, China. *Frontiers in Nutrition, 9*, 1070223.
Zhao, C., Dong, H., Zhang, Y., & Li, Y. (2019). Discovery of potential genes contributing to the biosynthesis of short-chain fatty acids and lactate in gut microbiota from systematic investigation in E. Coli. *npj Biofilms and Microbiomes, 5*(1), 19.